J Mater Sci: Mater Electron (2017) 28:11046–11052
DOI 10.1007/s10854-017-6888-4

Room-temperature metal–insulator transition of MBE grown VO_2 film investigated by temperature dependent resistance and transmittance

Minhuan Wang[1] · Lele Fan[2] · Jiming Bian[1] · Dong Zhang[3] · Hongzhu Liu[1] · Hongjun Sun[1] · Yingmin Luo[1]

Received: 19 February 2017 / Accepted: 30 March 2017 / Published online: 5 April 2017

Abstract VO_2 films were grown on TiO_2 (001) substrate by a radio frequency (RF)-plasma assisted oxide molecular beam epitaxy. An excellent reversible metal-to-insulator (MIT) transition accompanied with an abrupt change in both resistivity and infrared transmittance was observed at room temperature (RT), which was much lower than the 341 K for bulk single crystal VO_2. Remarkably, the MIT transition temperature (T_{MIT}) deduced from resistivity-temperature curve was well consistent with that obtained from the temperature dependent IR transmittance. The lowed T_{MIT} was supposed to be originated from the internal stress induced by the interface lattice mismatch between VO_2 film and TiO_2 substrate, this assumption was supported by both Raman measurement and X-ray diffraction (XRD) 2theta peak shift. This achievement will potentially open up new opportunities for advanced applications of VO_2-based devices where RT MIT is necessary.

1 Introduction

By virtue of its unique and fascinating properties, VO_2 was considered to be one of the key materials for a wide range of energy-related applications [1, 2]. It undergoes an abrupt reversible phase transition, known as metal-to-insulator transition (MIT) or semiconductor-to-metal (SMT) first-order transition. At temperatures below the transition temperature (T_{MIT}), VO_2 is in semiconducting state with monoclinic structure (space group $P2_1/c$), in which the V atoms pair open an energy gap of 0.6 eV. While at temperatures above T_{MIT}, VO_2 is in metallic state with rutile-tetragonal structure (space group $P4_2/mnm$), in which overlap between the Fermi level and the V_{3d} band eliminates the band gap [3]. Most notably, this allotropic transition in crystal symmetry and electronic band structure, which can be triggered by some specific external stimuli such as temperature or voltage, was usually accompanied by an abrupt and dramatic change in physical properties. For example, the electrical resistance jumps up to four orders of magnitude and the optical transmission shows a distinct switching effect especially within the infrared wavelength region across the MIT boundary. With these unique and fascinating properties, VO_2 was considered to be one of the most promising energy-saving material for a wide range of energy-related applications, including smart windows for energy utilization, supercapacitors for energy storage, and thermoelectric generators for energy conversion. However, the intrinsic T_{MIT} for bulk single crystals VO_2 has been well accepted to be ~341 K, the specific applications will be seriously limited by the relatively rigid T_{MIT} [4]. Successfully modulating the T_{MIT} to room temperature(RT) has been a long-standing research topic. For quite a long time, intentionally impurity doping had been commonly attempted to achieve controllable T_{MIT} since both shifts towards lower and higher temperature can be realized by selecting appropriate dopant and ratios, i.e., doping with high-valent metal cations (such as W^{6+},Nb^{5+},Mo^{6+}) were reported to lower the T_{MIT}, while doping with low-valent metal cations (such as

✉ Jiming Bian
jmbian@dlut.edu.cn

[1] Key Laboratory of Materials Modification by Laser, Ion and Electron Beams (Ministry of Education), School of Physics, Dalian University of Technology, Dalian 116024, China

[2] Key Laboratory for Advanced Technology in Environmental Protection of Jiangsu Province, Yancheng Institute of Technology, Yancheng 224051, China

[3] New Energy Source Research Center, Shenyang Institute of Engineering, Shenyang 110136, China

Al^{3+}, Ga^{3+} and Cr^{3+}) were expected to increase the T_{MIT} [4]. Nevertheless, the intentionally impurity doping generally suffered from the concomitant deterioration in change magnitude of electrical and optical characteristics as well as broadened hysteresis width, which was certainly undesirable for its practical applications as smart materials. Thus, the most critical challenge for VO_2 material lies in finding an effective and convenient way to reduce the T_{MIT} to room temperature while maintaining its abrupt MIT transition.

Recently, there has been a growing interest in modulating MIT behaviors of VO_2 films through internal stress since a relatively large T_{MIT} dependence on uniaxial stress along the c axis was proposed theoretically, which might be the most effective way to decrease the T_{MIT} due to its inherent advantages for many practical applications [5, 6]. Following this idea, the MIT process of the MBE grown VO_2 films was modulated continuously via the interfacial strain in our recent report [2]. However, there has been little investigation on the intimate correlation between electrical and optical properties across the MIT, which may shed light on the mechanism responsible for the specific MIT behavior in VO_2 film, for which no consensus has been reached.

In this study, VO_2 films with superior crystalline quality and ideal chemical stoichiometry were grown on TiO_2 (001) substrate by oxide molecular beam epitaxy (O-MBE). A systematical analysis were made on the crystal structure, morphology, electrical transport and transmittance within the infrared region (IR) of the VO_2 film. The results indicated that the RT MIT performance with narrow hysteresis width and large amplitude contrast in both IR optical transmittance and resistivity was realized, and the T_{MIT} deduced from resistivity–temperature curve was well consistent with the one obtained from the temperature dependent infrared (2 μm) transmittance. Our results will be favorable for exploit the advanced device applications based on VO_2 film working near RT [2, 7].

2 Experimental details

VO_2 films were grown on single crystal TiO_2 (001) substrate by a radio frequency (RF)-plasma assisted MBE with a base pressure better than 5.5×10^{-7} Pa. The details of the epitaxial film preparation have been reported elsewhere [2, 3]. The rutile TiO_2 single crystal is selected as substrate due to its stable thermal properties and the same crystal structure and space group as that of VO_2 film in high temperature tetragonal metallic phase. In addition, the measurements of electrical and optical properties across the MIT of VO_2 will not be affected considering the insulating and transparent characteristics of TiO_2 substrate. The TiO_2 (001) substrates with the dimensions of $10\times10\times0.5$ mm^3 were thoroughly cleaned to remove surface contamination and provide a atomically smooth surface for epitaxy deposition of VO_2 film. All the growth parameters, including the substrate temperature, the chamber pressure, the metallic vanadium evaporation rate and growth duration time, have been optimized for high crystalline quality and abrupt high magnitude MIT property. After deposition, the samples were cooled down to RT under the same oxygen pressure.

The crystallographic properties were determined by X-ray diffraction (XRD) using a LabXRD-6000 ($CuK_{\alpha1}$:$\lambda=0.154056$ nm). The surface morphology was examined by atomic force microscopy (AFM) with tapping mode using MI PicoScan 2500. The MIT properties were investigated by monitoring the change in both electrical resistivity and infrared transmittance across the MIT process, i.e., the samples were thermally cycled in the temperature ranging from 10 to 45 °C. The resistivity–temperature (R–T) behavior was investigated by measuring the electrical resistivity during heating and cooling process using the conventional electrical method by Keithley 2635 A source meter with 4-probe configuration. The temperature dependent infrared transmittance was studied by detecting the transmittance in the wavelength ranging from1400 to 5000 nm using a FT-IR FTIR SPECTROMETER (Bruker EQUINDX 55), and the transmittance in 2 μm wavelength was recorded as a function of temperature. The films composition and valence state of V were investigated by X-ray photoelectron spectroscopy (XPS) analyses on Thermo Scientific ESCALAB250Xi system with an $Al_{K\alpha}$ 1486.8 eV X-ray radiation source under a base pressure of 3×10^{-8} Pa. Before measurement, the sample was sputtered by Ar ion bombardment for 30 s for surface cleaning. The $O1_s$ binding energy line at 530 eV was taken as a reference for calibration and the composition was calculated from the peaks areas taking into account the sensitivity factors. Raman spectra measurements were carried out on DXR Raman Microscope with a 532 nm excitation laser source.

3 Results and discussion

Figure 1a shows the typical XRD patterns of the VO_2 film grown on single crystal TiO_2 (001) substrate by MBE under optimized conditions. For comparison, the XRD patterns of high quality VO_2 film (~60 nm) grown on c-plane sapphire substrate were also present in Fig. 1a, which exhibit MIT properties very close to bulk single crystal VO_2 material according to our previous experiments [8]. In addition to the dominant diffraction peaks corresponding to the TiO_2 substrate, the well-defined XRD diffraction peak corresponding to the VO_2 (002) was observed at 65.6° (JCPDS 76–0675) [9]. It should be noted that the growth of high quality pure phase VO_2

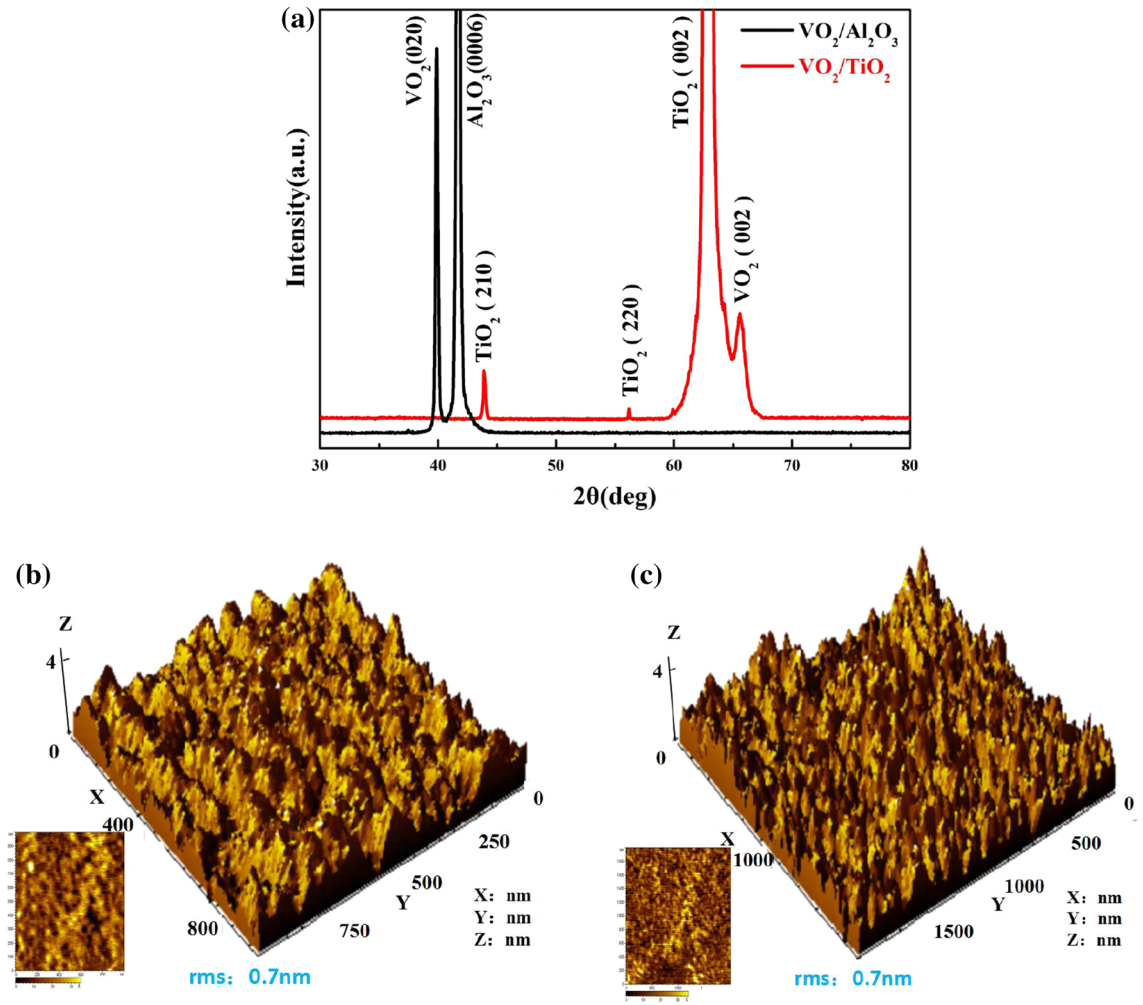

Fig. 1 **a** XRD patterns of VO_2 film grown on TiO_2 (001) substrate by MBE. For comparison, the XRD patterns of high quality VO_2 film grown on c-plane sapphire substrate were also present in Fig. 1, which exhibit MIT properties very close to bulk single crystal VO_2 material. **b** and **c** show the surface morphology AFM images of as-grown VO_2 film with the scanning area of (1 × 1 μm2) and (2 × 2 μm^2), respectively

film was still rather challenging due to the complexity of the vanadium-oxygen system [10]. Here, however, the high quality pure monoclinic phase VO_2 films with (002) preferred orientation have been achieved by MBE based on our previous optimization process [3, 8]. Comparing with the lower XRD profile, the only difference lies in the preferred orientation of VO_2 films, which was no doubt resulted from the induction of TiO_2 substrate. Because it was very likely that very thin VO_2 films (around 30 nm for current case) below a critical thickness are constrained to have the same lattice structure as the tetragonal TiO_2 (001) substrate. Here, the critical thickness refers to the thickness at which the misfit dislocations are generated to relax the film and form the equilibrium phase. It has been demonstrated that the phase transformation and strain relaxation phenomena follow totally different kinetics in thin and thick layers [10]. In addition, according to Bragg equation: $2d\sin\theta = n\lambda$, where the d is crystal plane spacing, θ is incident angle, n and λ are integers and constants, respectively. The slightly shift in VO_2 (002) 2θ angle compared with the value for single crystal VO_2 material (JCPDS 76-0675), indicating a smaller crystal plane spacing d and thus implying the existence a tensile stress in-plane mainly originated from the misfit between VO_2 film and TiO_2 substrate. Moreover, the surface morphology of the VO_2 film is illustrated by AFM measurements. The AFM images with the scanned area of 1 × 1 μm^2 and 2 × 2 μm^2 were shown in the Fig. 1b, c, respectively. As can be seen from these images, the sample exhibit smooth and homogeneous surface morphology composed of uniformly and dense grains with spherical granular crystallites, and the same

root mean square (rms) was observed to be 0.7 nm for both images. While the uniform and dense nano columns are more clearly visible in the images of Fig. 1c.

The XPS measurements were carried out to identify the valence state of V in the VO_2/TiO_2 structure (Fig. 2). The XPS survey spectra was shown in Fig. 2a, all the elements can be well identified in the survey spectra according to previous reports in literature [11, 12]. The detected signal from $C1_s$ could be attributed to unintentionally contamination from ambient during the growth and measurement process since C element was ubiquitous element in the environment. To identify the precise valence state of V in the oxide layer, the enlarged high-resolution XPS spectra focusing on $V2_{p3/2}$ and $O1_s$ with binding energy between 510 and 533 eV was shown in Fig. 2b. The $O1_s$ peak could be de-convoluted into two peaks, only the one at 530.0 eV

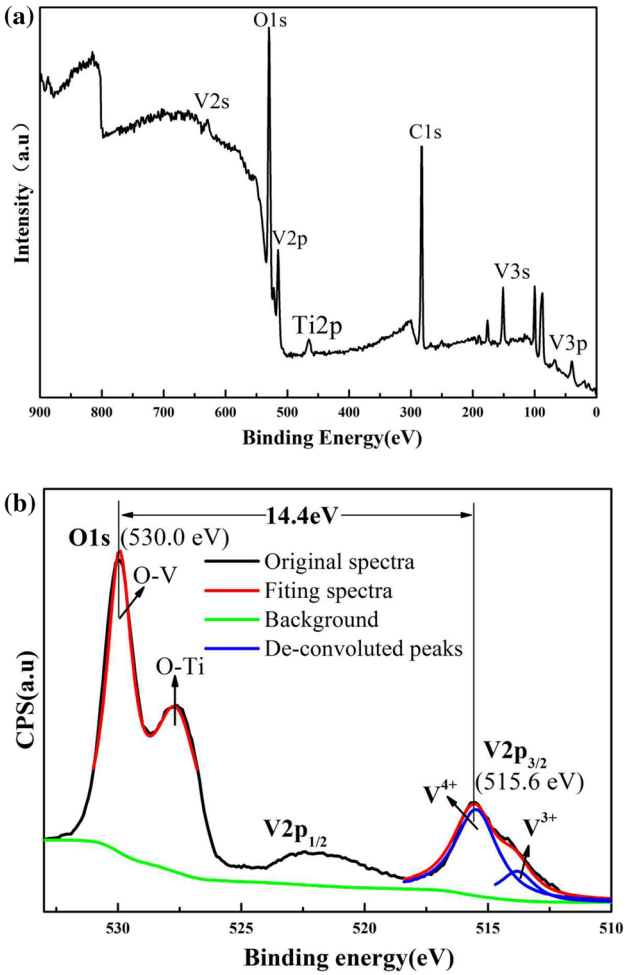

Fig. 2 **a** XPS survey spectra with binding energy in the range of 0-900 eV for VO_2/TiO_2 structure. **b** The enlarged high-resolution spectra with binding energy in the range of 510–533 eV and the fitting results for sample VO_2/TiO_2 heterostructure. After subtracting the Shirley background (*cyan curve*), the $V2p_{3/2}$ peak could be de-convoluted into V^{4+} and V^{3+} peaks

related to vanadium oxides, whereas the other peak at 527.8 eV comes from titanium oxide. Meanwhile, the typical two-peak structure ($V2_{p3/2}$ at 515.6 eV and $V2_{p1/2}$ at 523.3 eV) due to the spin–orbit splitting was observed for the V_{2p} signal. According to Silversmit's method, the binding energy span between $O1_s$ and $V2_{p3/2}$ core level could be utilized as a criterion to identify the different vanadium oxidation states, since it differs remarkably for VO_x with disparate valence state [11]. The calculated binding energy span from Fig. 2b was 14.4 eV, which was in rational agreement with the value of 14.35 eV for stoichiometric VO_2 epitaxial layer [13], suggesting that the valence state of V in as-grown VO_2 film was principally composed of V^{4+} [11]. Moreover, the slightly asymmetric feature of the $V_{2p3/2}$ peak suggests the existence of trace amount of V^{3+} in the VO_2 film. After subtracing the Shirley background (cyan) using Gaussian Lorentzian sum function by XPSPEAK 4.1 software, the $V2_{p3/2}$ peak could be de-convoluted into two peaks, i.e., V^{4+} peak at 515.6 eV and V^{3+} peak at 513.8 eV, no other valence state of V was detected. The oxygen deficiency during high vacuum growth might be responsible for the formation of V^{3+}. It should be noted that the commonly observed V^{5+} peak at ~517.0 eV, which are usually caused by the surface oxidization as a slighly oxygen rich composition generally exist only on the surfaces (the top several nanometers), was not detected in current case. It has been confirmed that the MIT characteristics might be seriously degraded by the existence of a small amount of vanadium oxides with different stoichiometric composition rather than VO_2, such as V_2O_3 or V_2O_5, which may exist at the surface or grain boundaries of VO_2 grains, although may not be detected by the XRD measurement [14, 15]. So the ideal stoichiometry composition was imperative for reliable material properties of VO_2 film. Here, the ratio of oxygen to vanadium can be roughly estimated to be 1.91 from the integrated area of $I_V{}^{4+}$ and $I_V{}^{3+}$ by the empirical formula: $(2I_V{}^{4+} + 1.5I_V{}^{3+})/(I_V{}^{4+} + I_V{}^{3+})$ [14], indicating the nearly stoichiometrical O/V ratio inside the prepared VO_2 film. Therefore, the super crystalline quality and ideal chemical stoichiometry of our MBE grown VO_2 film were clearly evidenced by XRD, AFM and XPS investigation.

The MIT performance of the as-grown VO_2 sample was investigated by the temperature dependent electrical resistivity and IR optical transmittance measurements across the MIT process. As shown in Fig. 3, an excellent reversible MIT phase transition accompanied with an abrupt change in both electrical resistivity and IR optical transmittance was observed, and the smooth transition profiles suggesting a first-order reversible MIT behavior for the VO_2 film grown on TiO_2 (001) substrate. The differential d(R)/d(T) versus temperature curves for heating and cooling branches were shown in the left bottom of Fig. 3a, and the T_{MIT} can be determined from the Gaussian fit of the d(R)/dT curves

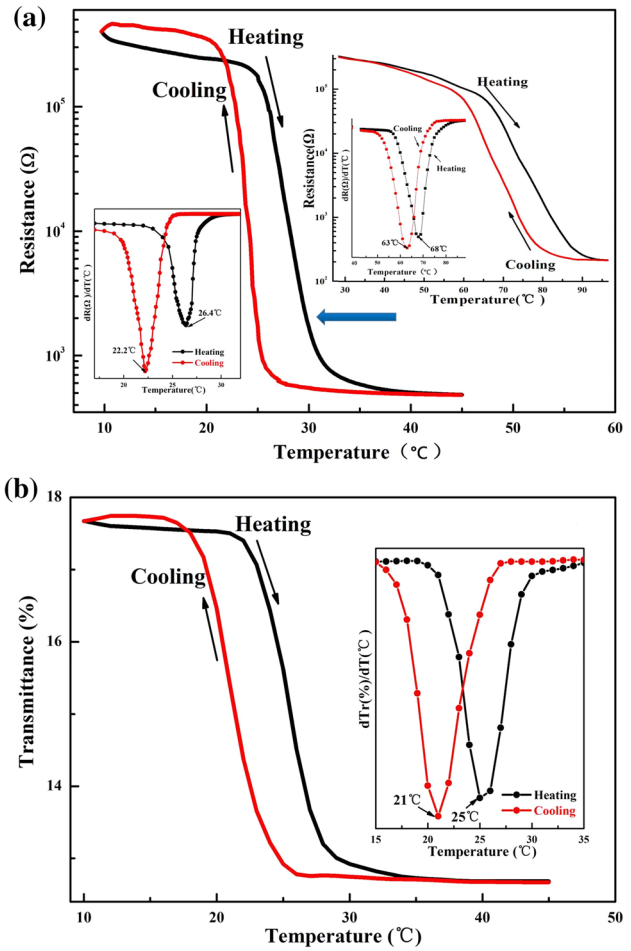

Fig. 3 **a** Thermal hysteresis loops of resistance for the VO_2 film grown on TiO_2(001) substrate by MBE. For comparison, the thermal hysteresis loops for the VO_2 film grown on sapphire substrate were shown on the *top right corner*. The differential d(R)/d(T) versus temperature curves were shown in the corresponding insets. **b** Thermal hysteresis loops of IR transmission at 2 μm wavelength for VO_2 film grown on TiO_2 (001) substrate. The differential d(Tr)/d(T) versus temperature curves were shown in the *inset* to determine the T_{MIT}

(at which the value reach its extremum). For comparison, the result for the VO_2 film grown on c-plane sapphire substrate, which exhibit MIT properties very close to bulk single crystal VO_2 material according to our previous report [8], were also shown in the top right corner of Fig. 3a. The MIT properties can be characterized by the following parameters: T_{MIT} (defined as peak temperature for both heating and cooling runs), ΔH (MIT thermal hysteresis width, defined as the difference of T_{MIT} for heating and cooling branch), ΔT (MIT sharpness, characterized by the FWHM of the derivative curve of dR/dT-T plot), as well as ΔA (MIT amplitude, defined as ratio of resistivity in insulator phase to that in metallic phase in the heating process). So it can be seen that the T_{MIT} show remarkable shift towards lower temperature, i.e., 68 °C for previous VO_2 film on c-plane sapphire substrate while RT (26 °C) for current VO_2 film on TiO_2 (001) substrate. While other MIT parameters (including ΔH, ΔT, and ΔA) remains almost on the same orders of magnitude as that in the top right corner of Fig. 3a, suggesting the distinct abrupt MIT performance was maintained perfectly during the decrease of T_{MIT} to RT. The relatively large MIT amplitude of exceeding three orders of magnitude and a narrow hysteresis width will be especially imperative for switching-type applications. Generally extremely demanding processing conditions are required for VO_2 films with lowered T_{MIT} and abrupt MIT behavior [8]. So the MIT investigation further confirming the high crystalline quality and phase purity of current VO_2 film, which was in well agreement with above XRD, AFM and XPS analysis. Moreover, the IR transmittance at 2 μm wavelength was recorded during heating and cooling process as shown in Fig. 3b, and the differential d(Tr)/d(T) (Tr stands for transmittance) versus temperature curves were shown in the insets of Fig. 3b. The T_{MIT} determined from the Gaussian fit of the d(Tr)/dT curves was 25 °C. Remarkably, the rather small hysteresis width was comparable with the high quality stoichiometric VO_2 film grown on c-plane sapphire substrate, which will be especially favorable for rapid response to environmental temperature as thermochromic smart window application. Therefore, the T_{MIT} and hysteresis width deduced from R–T curve (Fig. 3a) was well consistent with the one obtained from the temperature dependent infrared (2 μm) transmittance(Fig. 3b).

According to theoretical prediction, the observed remarkable decrease of T_{MIT} should be closely related with the internal stress induced by the interface lattice mismatch between TiO_2 substrate and VO_2 film [2]. Herein, the Raman spectra measurements were carried out since the line shape of Raman spectrum was extremely sensitive to the residual stress inside the films. For comparison, the Raman spectra for high quality VO_2 film with fully relaxed stress were also present with black line, which exhibit peaks very close to bulk single crystal VO_2 material according to our previous experiments [8]. As can be seen from Fig. 4, all the main peaks can be well indexed to the monoclinic VO_2, especially the Raman peak at 617 cm^{-1} (which can be regarded as the signal of M–VO_2) was quite pronounced, indicating that the high quality single phase VO_2 films were obtained on TiO_2 substrate [16]. Moreover, a slight red shift in the main peaks indicating an in-plane tensile stress due to the lattice mismatch, which was also supported by the XRD 2theta peak shift as mentioned above. As expected from Poisson effect (shown in the inset of Fig. 4a, as the VO_2 film was stretched in plane, it would tend to be compressed out-of-plane, i.e., in the direction perpendicular to the direction of expansion. Fig. 4b, c show the schematic diagram of microscopic structure of the epitaxy

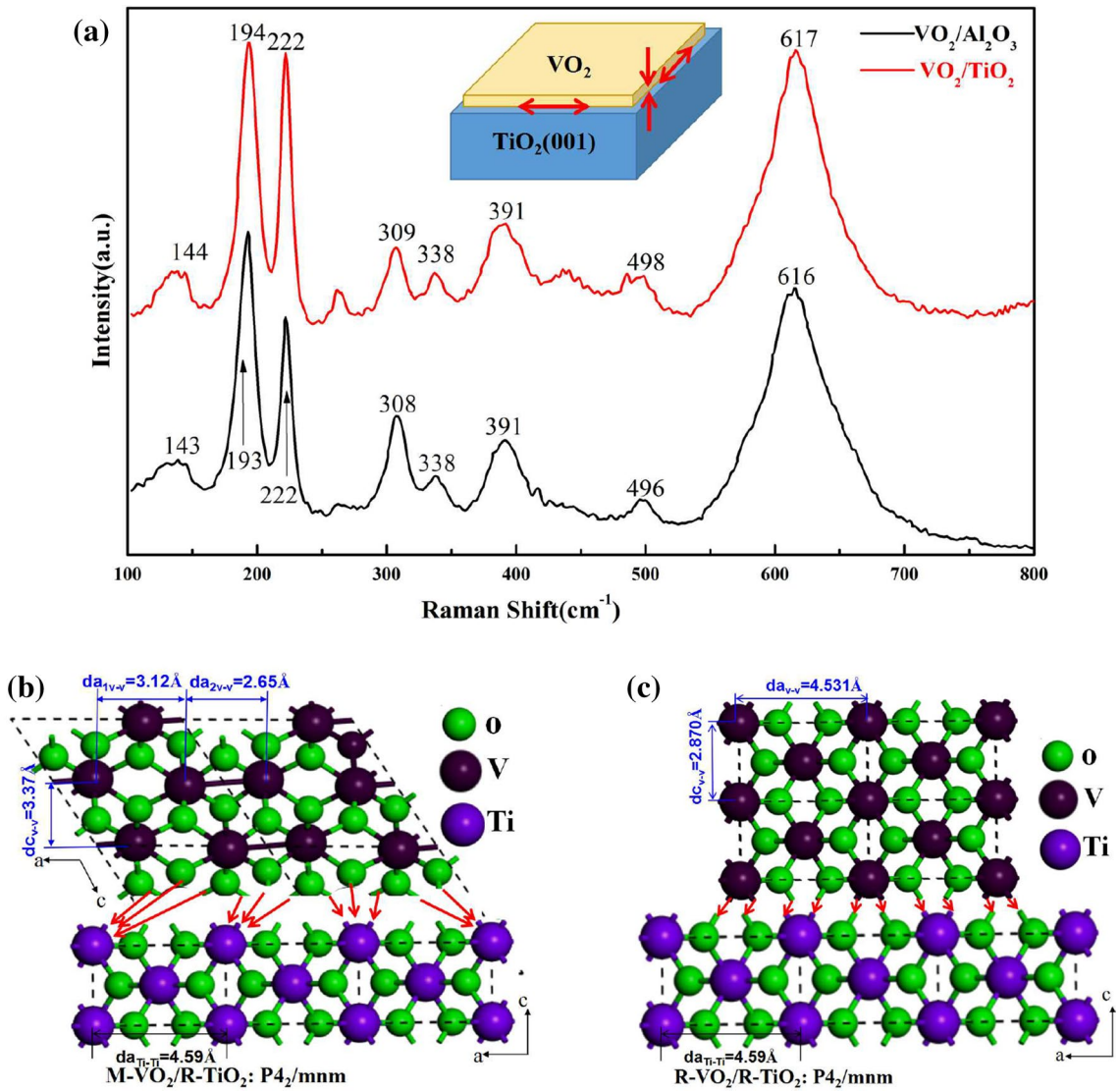

Fig. 4 **a** The Raman spectra for VO_2 film grown on TiO_2(001) substrate by MBE(*red line*). For comparison, the Raman spectra for high quality VO_2 film with fully relaxed stress were also present with *black line*. **b** and **c** show the schematic diagram of microscopic structure of the VO_2(002)/TiO_2(001) interface with VO_2 in monoclinic ($T < T_{SMT}$) and tetragonal ($T > T_{SMT}$) structure, respectively. (Color figure online)

VO_2 (002)/TiO_2 (001) interface with VO_2 in monoclinic ($T < T_{MIT}$) and tetragonal ($T > T_{MIT}$) structure. And the lattice parameters of VO_2 and TiO_2, together with the corresponding lattice mismatch between them were listed in Table 1. Since the lattice parameters of VO_2 are smaller than those of TiO_2 in both forms, the in-plane tensile stress will be generated for the epitaxially grown VO_2 films on TiO_2(001) substrate due to the lattice mismatch, further leading to compression along c-axis according to the well-known Poisson's relation. This was in well consistent with above Raman analysis. Furthermore, as the temperature is lower than the T_{MIT} Fig. 4b, a very large mismatch up to 25% across the $VO_2^{monincial}$/$TiO_2^{tetragonal}$ interface could be obtained. While as the temperature exceeds the T_{MIT} (Fig. 4c), only a tiny lattice mismatch exist across the $VO_2^{tetragonal}$/$TiO_2^{tetragonal}$ interface due to the similar tetragonal structure of rutile phase VO_2 and TiO_2. The reduced V^{4+}–V^{4+} distance in the crystal structure results in direct overlapping of d orbitals, which stabilized the metallic phase of the rutile structure. In other words, the residual compressive stresses can counteract the transition energy barriers and stimulate the occurrence of the MIT sharply. In addition, the trace amount of V^{3+} caused by the oxygen deficiency during high vacuum growth might also partially contributes to the decrease of T_{MIT} [2].

Table 1 The lattice parameters of VO_2 and TiO_2 in monoclinic and rutile form, together with the corresponding lattice mismatch between them

Material	Space group	Lattice parameter				Lattice mismatch			
		a (Å)	b (Å)	c (Å)	β (°C)	a (%)	b (%)	c (%)	β (%)
VO_2	Monoclinic P_{21}/c	5.74	4.52	5.38	122.6	25.05	1.525	81.75	36.22
VO_2	Rutile $P4_2/mnm$	4.53	4.53	2.87	90	1.307	1.307	3.041	0
TiO_2		4.59	4.59	2.96	90				

4 Conclusion

In summary, the VO_2 film with superior crystalline quality and ideal chemical stoichiometry was grown on TiO_2 (001) substrates. An excellent RT reversible MIT performance was observed with an abrupt change in both resistivity and infrared optical transmittance. Remarkably, the T_{MIT} deduced from R–T curve was well consistent with the one obtained from the temperature dependent infrared (2 μm) transmittance. Based on the Raman measurement and microstructure model, the RT MIT properties was mainly attributed to the residual compressive stresses imposed by the TiO_2 (001) substrates. Our achievement will potentially open new opportunities for advanced applications of VO_2-based devices.

Acknowledgements We acknowledge support from the Fundamental Research Funds for the Central Universities (DUT16LAB11), NSFC (61520106013).

Compliance with Ethical Standards

Conflict of interest The authors declare that they have no potential conflict of interest to this work.

References

1. J.H. Park, J.M. Coy, T.S. Kasirga, C.M. Huang, Z.Y. Fei, S. Hunter, D.H. Cobden, Nature **500**, 431 (2013)
2. L.L. Fan, S. Chen, Z.L. Luo, Q.H. Liu, Y.F. Wu, L. Song, D.X. Ji, P. Wang, W.S. Chu, C. Gao, C.W. Zou, Z.Y. Wu, Nano Lett. **14**, 4036 (2014)
3. M.H. Wang, J.M. Bian, H.J. Sun, H.Z. Liu, X.X. Li, Y.M. Luo, H.L. Huang, Y.Z. Zhang, J. Mater. Sci. **51**, 8233 (2016)
4. S.F. Wang, M.S. Liu, L.B. Kong, Y. Long, X.C. Jiang, A.B. Yu, Prog. Mater. Sci. **81**, 1 (2016)
5. Y. Muraoka, Z. Hiroi, Appl. Phys. Lett. **80**, 583 (2002)
6. K. Martens, N. Aetukuri, J. Jeong, M.G. Samant, S.P. Parkin, Appl. Phys. Lett. **104**, 081918 (2014)
7. K.K. Nagashima, T.S. Yanagida, H.K. Tanaka, Phys. Rev. B **74**, 172106 (2006)
8. J.M. Bian, M.H. Wang, H.J. Sun, H.Z. Liu, X.X. Li, Y.M. Luo, Y.Z. Zhang, J Mater. Sci. **51**, 6149 (2016)
9. M.R. Bayati, R. Molaei, F. Wu, J.D. Budai, Y. Liu, R.J. Narayan, J. Narayan, Acta Mater. **61**, 7805 (2013)
10. C.Z. Wu, F. Feng, Y. Xie, Chem. Soc. Rev **42**, 5157 (2013)
11. Y.X. Guo, Y.F. Liu, C.W. Zou, Z.M. Qi, Y.Y. Wang, Y.Q. Xu, X.L. Wang, F. Zhang, R. Zhou. Appl. Phys. A. **115**, 1245 (2014)
12. K. Zhao, L.T. Teng, Y.F. Tang, X. Chen. Ceram. Int. **40**, 15335 (2014)
13. J. Mendialdua, R. Casanova, Y. Barbaux, J. Electron Spectrosc. Relat. Phenom. **71**, 249 (1995)
14. Y. Zhou, S. Ramanathan, J. Appl. Phys **112**, 074114 (2012)
15. Z. Yang, C. Ko, S. Ramanathan, J. Appl. Phys. **108**, 073708 (2010)
16. F.H. Chen, L.L. Fan, S. Chen, G.M. Liao, Y.L. Chen, P. Wu, L. Song, C.W. Zou, Z.Y. Wu, ACS Appl. Mater. Interfaces **7**, 6875 (2015)